

Recent extreme drought events in the Amazon rainforest: Assessment of different precipitation and evapotranspiration datasets, and drought indicators

Phillip Papastefanou¹, Christian S. Zang², Zlatan Angelov¹, Aline Anderson de Castro³, Juan Carlos Jimenez⁴, Luiz Felipe Campos De Rezende³, Romina Ruscica^{5,6,7}, Boris Sakschewski⁸, Anna Sörensson^{5,6,7}, Kirsten Thonicke⁸, Carolina Vera^{5,6,7}, Nicolas Viovy⁹, Celso Von Randow³ and Anja Rammig¹

¹Technical University of Munich, TUM School of Life Sciences Weihenstephan, Freising, Germany

²University of Applied Sciences Weihenstephan-Triesdorf, Department of Forestry, Freising, Germany

³Earth System Sciences Centre, National Institute for Spatial Research, São José dos Campos, São Paulo, Brazil

⁴GCU/IPL, University of Valencia, Valencia. Spain.

⁵Universidad de Buenos Aires, Facultad de Ciencias Exactas y Naturales, Departamento de Ciencias de la Atmósfera y los Océanos. Buenos Aires, Argentina.

⁶CONICET – Universidad de Buenos Aires. Centro de Investigaciones del Mar y la Atmósfera (CIMA). Buenos Aires, Argentina.

⁷CNRS – IRD – CONICET – UBA. Instituto Franco-Argentino para el Estudio del Clima y sus Impactos (UMI 3351 IFAECI). Centro de Investigaciones del Mar y la Atmósfera (CIMA). Buenos Aires, Argentina.

⁸Potsdam Institute for Climate Impact Research (PIK), Telegraphenberg A31, Potsdam, 14473, Germany

⁹LSCE, CEA-CNRS-Univ Paris-Saclay, Saclay, France

Correspondence to: Phillip Papastefanou (papa@tum.de)

23 **Abstract**

24 Over the last decades, the Amazon rainforest was hit by multiple severe drought events. Here, we assess the severity and spatial
25 extent of the extreme drought years 2005, 2010, and 2015/2016 in the Amazon region and their impacts on the regional carbon
26 cycle. As an indicator of drought stress in the Amazon rainforest, we use the widely applied maximum cumulative water deficit
27 (MCWD). Evaluating nine state-of-the-art precipitation datasets for the Amazon region, we find that the spatial extent of the
28 drought in 2005 ranges from 2.2 to 3.0 (mean = 2.7) million km² (37 – 51% of the Amazon basin, mean = 45%) where MCWD
29 indicates at least moderate drought conditions (relative MCWD anomaly < -0.5). In 2010, the affected area was about 16%
30 larger, ranging from 3.0 up to 4.4 (mean = 3.6) million km² (51 – 74%, mean = 61%). In 2016, the mean area affected by
31 drought stress was between 2005 and 2010 (mean = 3.2 million km²; 55% of the Amazon basin), but the general disagreement
32 between datasets was larger, ranging from 2.4 up to 4.1 million km² (40–69%). In addition, we compare differences and
33 similarities among datasets using the self-calibrating Palmer Drought Severity Index (scPDSI) and a rainfall anomaly index
34 (RAI). We find that scPDSI shows a stronger, and RAI a much weaker drought impact in terms of extent and severity for the
35 year 2016 compared to MCWD. We further investigate the impact of varying evapotranspiration on the drought indicators
36 using two state-of-the-art evapotranspiration datasets. Generally, the variability in drought stress is most dependent on the
37 drought indicator (60%), followed by the choice of precipitation dataset (20%) and the evapotranspiration dataset (20%). Using
38 a fixed, constant evapotranspiration rate instead of variable evapotranspiration can lead to an overestimation of drought stress
39 in the parts of Amazon basins that have a more pronounced dry season (for example in 2010). We highlight that even for well-
40 known drought events the spatial extent and intensity can strongly depend upon the drought indicator and the data sources it
41 is calculated with. Using only one data source and drought indicator has the potential danger to under or overestimate drought
42 stress in regions with high measurement uncertainty, such as the Amazon basin.

Formatted: Header

Formatted: Justified, Line spacing: 1,5 lines

Deleted: We conclude that for investigating impacts of droughts on the Amazon rainforest and e.g. its carbon cycle, multiple datasets for precipitation and also variable evapotranspiration input should be considered. Furthermore, considering different drought indices can help to understand the complex characteristics that drought events in the Amazon have.

Formatted: Font: Not Bold, Font colour: Auto

1 Introduction

The severe drought events occurring in 2005, 2010, and 2015/16 in the Amazon basin are reasons for concern regarding their frequency and severity, and their impacts on the Amazon rainforest. Different large-scale atmospheric processes related to increased sea surface temperature (SST) in the Pacific and the Atlantic Ocean seem to be responsible for such repeated megadrought events (Coelho et al., 2012): While the drought 2015/16 was driven by a record-level El Niño event enhanced by the strong underlying global warming trend (Jimenez et al., 2018), the 2010 drought was a combination of a moderate El Niño event and anomalously warm SSTs in the tropical North Atlantic (Marengo et al., 2011; Marengo & Espinoza, 2016). Similarly, the 2005 drought was attributed to anomalies of warm SSTs in the North Atlantic (Marengo, Nobre, Tomasella, Oyama, et al., 2008; Zeng et al., 2008). In consequence, such events differ in their strength, their timing, and spatial patterns, and thus, impacted regions differ. While drought events related to El Niño events show a Southwest to Northeast gradient with dry conditions over the NE Amazon region (Malhi et al., 2008), drought events caused by anomalously warm North Atlantic SSTs show a North-South gradient with dry conditions in the southern Amazon region (Lewis et al., 2011; Marengo et al., 2008). Even in the case of El Niño events, SSTs anomalies over the Eastern Pacific (EP) or the Central Pacific (CP) can lead to different impacts and spatial patterns of drought (Jimenez et al., 2019). In addition to their influence on temperature, recent El Niño events also showed amplified atmospheric vapor pressure deficit anomalies (Barkhordarian et al., 2019; Rifai et al., 2019). The impacts of such drought events on humid tropical forests, which are often not adapted to longer-lasting dryness, are severe. Increased forest mortality connected to drought events was observed in central and southern Amazonia (Feldpausch et al., 2016; Lewis et al., 2011; Phillips et al., 2009), as well as shifts in tree species composition (Esquivel-Muelbert et al., 2019). Droughts are assumed to be one of the main drivers for the observed decline in the Amazon carbon sink, indicating that more carbon is lost to the atmosphere than taken up by the forest (Hubau et al., 2020). Thus, such extreme drought events are altering the carbon cycle of the Amazon forest (Feldpausch et al., 2016; Gloor et al., 2015; Hubau et al., 2020; Phillips et al., 2009).

Losing tropical forests in the Amazon region through increased mortality under drought also has implications for regional and continental scale water cycling (Ruiz-Vásquez et al., 2020). The rainforest transpires enormous amounts of water which is transported by winds to remote regions far beyond the borders of the rainforest (e.g. Dirmeyer et al., 2009; van der Ent et al., 2010; Zemp et al., 2014, 2017). In addition, the ongoing deforestation in the Amazon rainforest further decreases forest cover and thus, transpiration rates, leading to a rainfall decline and enhanced drought conditions in a positive feedback loop (Miralles et al., 2019; Zemp et al., 2017). It can be expected that ongoing climate change most likely will cause stronger and more frequent drought events in the Amazon (Cai et al., 2015; Jiang et al., 2020; Marengo & Espinoza, 2016).

For assessing the severity, the spatial extent, and, in particular, the impacts of such drought events on existing ecosystems, different gridded precipitation datasets are available which in some cases differ strongly in magnitude and spatio-temporal distribution of precipitation amounts (Golian et al., 2019). Typical problems of precipitation data for South America encompass the underestimation of extreme rainfall events in both dry or wet seasons (Blacutt et al., 2015; Giles et al., 2020). Therefore, while for the Amazon region, the recent drought events have been assessed in terms of severity (Jimenez et al., 2018; Jiménez-

Formatted: Header

Formatted: Font: Not Bold, Font colour: Auto

Formatted: Space Before: 0 pt, After: 0 pt, Line spacing: 1,5 lines, Don't keep with next, Border: Top: (No border), Bottom: (No border), Left: (No border), Right: (No border), Between : (No border)

Muñoz et al., 2016) and impacts (Feldpausch et al., 2016; Lewis et al., 2011; Phillips et al., 2009) based on single precipitation data sets, a systematic analysis of how the most frequent used precipitation datasets differ regarding the spatial extent, location and severity of recent extreme drought events, is currently missing.

For our study, we selected precipitation from nine different datasets: (1, 2) Data from the Tropical Rainfall Measurement Mission (TRMM) version 6 and 7 (Huffman et al., 2007) which have been frequently used, e.g. to estimate drought impacts on the carbon balance (Lewis et al., 2011; Malhi et al., 2009) and are assumed to represent precipitation patterns in the Amazon region best since they are derived from radar measurements (Huffman et al., 2007). (3) CHIRPS (Climate Hazards group Infrared Precipitation with Stations, Espinoza et al., 2019), which has been used to study regional hydro-climatic and environmental changes in the Amazon Basin. These two datasets only provide precipitation and no information about other climatic variables such as temperature or radiation. In addition, we selected five datasets that are often used as drivers for ecosystem models (e.g. in Forkel et al., 2019; Yang et al., 2015) and – in contrast to the other datasets – provide information for more climate variables: Data from the Climate Research Unit (CRU) with a joint project reanalysis (NCEP, National Centers for Environmental Prediction) applied, (4) the CRUNCEP (version 8, Viovy, 2018), (5) the WATCH-WFDEI (WATCH: Water and Global Change, Weedon et al., 2011). WFDEI: WATCH Forcing Data methodology applied to ERA-Interim, Weedon et al., 2014) dataset, originally derived from global sub-daily observations merged with integrations from a general circulation model, (6) the GSWP3 (Global Soil Wetness phase 3, Kim et al. in prep) dataset which is closely related to WATCH-WFDEI, relying on a similar forcing but with a different bias-correction method applied, (7) the newer GLDAS (Global Land Data Assimilation System) 2.1. which is derived from various geostationary infrared satellite measurements and microwave observations (Rodell et al., 2004), (8) the latest ECMWF atmospheric reanalysis dataset, ERA5, which is the successor of ERA-Interim, providing higher spatial and temporal resolutions and a more recent model and data assimilation system than the previous ERA-Interim reanalysis (Albergel et al., 2018), and, finally, (9) the GPCC (named after the Global Precipitation Climatology Centre) dataset (Schneider et al., 2018), which is based on globally available land stations (rain gauges) combined with an empirical interpolation method (Willmott et al., 1985). The data sets were chosen because they are often used to force Dynamic Global Vegetation and hydrological simulation models in climate impacts studies. A more detailed description of the datasets is given in the methods section.

We evaluate the precipitation datasets based on the Maximum Cumulative Water Deficit (MCWD; Aragão et al., 2007), a well-established drought index that is particularly suitable for estimating drought stress in the Amazon region (e.g. Esquivel-Muelbert et al., 2019; Lewis et al., 2011; Malhi et al., 2009; Phillips et al., 2009; Zang et al., 2020). In addition, we included two other measures to complement our analysis: A rainfall anomaly index (RAI), which does account for the mean deviation (in units of standard deviation) of precipitation during the driest months of the year, and the scPDSI (self-calibrating Palmer Drought Index, Wells et al., 2004). The scPDSI index has a more complex formulation compared to RAI and MCWD and takes available soil water content into account. Both RAI and scPDSI have been used in studies describing the recent Amazonian drought events (e.g. Jiménez-Muñoz et al., 2016; Lewis et al., 2011). Many studies (e.g. Flack-Prain et al., 2019; Hubau et al., 2020) currently still use a fixed evapotranspiration rate for the calculation of MCWD instead of using

118 evapotranspiration datasets as input. To assess the robustness of a fixed evapotranspiration rate, we include two
119 evapotranspiration datasets GLEAM (Martens et al., 2017) and DOLCE (Hobeichi et al., 2018) for the calculation of MCWD
120 and scPDSI. The goals of our study are (1) to analyse and quantify the uncertainty in strength, extent, and location of three
121 recent Amazon droughts in the years 2005, 2010, and 2015/2016 in precipitation from nine state-of-the-art precipitation or
122 climate datasets based on MCWD; (2) to examine differences among these drought events by taking two additional drought
123 indicators RAI and scPDSI and two evapotranspiration datasets into account.

2 Methods

2.1 Study area

Our study covers the Amazon river basin as delineated by Döll & Lehner (2002, see black contour in Fig. 1). Using 0.5° spatial resolution in longitude and latitude results in 1946 grid cells of interest for this study area. Note that differences in the comparison of our results with Lewis et al., (2011) arise because of differences in the delineation of the Amazon region, i.e. the area used in our study is 0.6 million km² larger.

2.2 Data sources

In the following, we briefly describe the nine precipitation datasets applied in our study (see also Table 1): The Tropical Rainfall Measuring Mission (TRMM v7) product (Huffman et al., 2007) is a precipitation-only dataset based on multiple microwave-infrared satellite data developed as a joint product between NASA and the Japan Aerospace Exploration Agency (JAXA). We also included the predecessor v6 for comparison in our study, because it has been frequently and prominently used to derive drought impacts to the Amazon Basin (e.g. Lewis et al., 2011; Phillips et al., 2009) and shows significantly lower precipitation throughout the basin compared to v7 (Seto et al., 2011). CHIRPS (Climate Hazards group Infrared Precipitation with Station) is a novel dataset (Funk et al., 2015) which is a quasi-global (full longitude, but only 50°S – 50°N latitude extent) precipitation-only merged product, based on multi-satellite estimates (similar to TRMM 6 and TRMM 7) and approx. 2,000 in-situ observations per month in South America. TRMM 6, TRMM 7 and CHIRPS share the quasi-global spatial extent, however, in comparison to TRMM 6, TRMM 7 with a resolution of 0.25° x 0.25°, CHIRPS has a much higher spatial resolution of 0.05° x 0.05°. ERA5 (Muñoz-Sabater et al., 2018) shows improvements in, e.g., land evapotranspiration, surface soil moisture and turbulent heat fluxes over its predecessor ERA-Interim (Albergel et al., 2018), which we decided not to include in our study as it showed higher systematic errors over tropical areas (Nogueira, 2020). Similarly, CRUNCEP (Viovy, 2018) is generated based on a reanalysis from the national centers for environmental prediction (NCEP) and the National Center for Atmospheric Research (NCAR), corrected with the CRU TS3.2 (Harris et al., 2014) dataset. GPCC is mainly based on data from rain-gauge land stations. Similar to CRUNCEP, it is also based on the NCEP reanalysis dataset and has been used in global drought studies (Ziese et al., 2014). Both GPCC and CRUNCEP cover the longest periods of all selected datasets in this study with time spans from 1891 until 2016 and from 1901 until 2016, respectively. WATCH-WFDEI (Weedon et al., 2011; 2014) is based on the reanalysis ERA-Interim corrected with GPCC precipitation. GSWP3 (Kim et al. in prep;) is based on the atmospheric reanalysis method “20CR” (20th Century Reanalysis version 2, Compo et al., 2013), which has been dynamically downscaled to 0.5° x 0.5° resolution. Corrections with observational data have not only been applied to precipitation but also to short/longwave radiation, air temperature and the daily temperature range. Both WATCH-WFDEI and GSWP end in the year 2010. The GLDAS 2.1 dataset is built by using the ‘Noah Land surface model’ forced by

the Goddard Earth Observing System (GEOS) Data Assimilation System with corrected precipitation and radiation (Rodell et al., 2004; Sheffield et al., 2006). Starting in January 2000 (Version 2.1), it is the dataset with the latest time onset and hence defines the lower-bound time interval considered in this study. For the 2015/2016 drought event, only seven datasets were available as three of the datasets (TRMM 6, GSWP3 and WATCH-WFDEI) end before. All datasets were (if not directly available) aggregated to $0.5^\circ \times 0.5^\circ$ spatial resolution and to monthly time steps.

2.3. Drought indices and evaluation of drought area and extent

2.3.1 Calculation of maximum climatological water deficit (MCWD)

We calculate MCWD based on Aragão et al. (2007) defining water deficit (WD) as follows:

$$WD(t) = \begin{cases} P(t) - ET(t) & \text{if } P(t) - ET(t) < 0 \\ 0 & \text{else} \end{cases} \quad (1)$$

where $WD(t)$ stands for water deficit, which is calculated for a time step t , in this case monthly, $P(t)$ for monthly precipitation and $ET(t)$ for monthly evapotranspiration. To estimate the impacts of persistent drought events, the cumulative water deficit (CWD) is defined as the accumulation of water deficit of each month of the hydrological year (see below for details) for which $P(t)$ is smaller than $ET(t)$, hence $WD(t)$ is negative. MCWD is the most negative value of $CWD(t)$ over a specific period.

As proposed by Aragão et al. (2007), we use a fixed value for $ET(t) = ET_{fixed} = 100 \text{ mm month}^{-1}$ derived from ground measurements of evapotranspiration in different locations and seasons in Amazonia (da Rocha et al., 2004; von Randow et al., 2004). As a result, water deficit builds up whenever monthly rainfall $P(t)$ falls below 100 mm.

We calculate annual MCWD for the hydrological year from October of the previous year to September of the succeeding year, e.g. the MCWD for the year 2005 is calculated from October 2004 to September 2005 (similar to Lewis et al., 2011). CWD

and consequently MCWD are reset after each hydrological year.

In contrast to e.g. Lewis et al. 2011, we use the relative MCWD anomaly (from now also denoted as $rMCWD$) as our main drought indicator. For deriving $rMCWD$, we estimate the absolute MCWD anomaly (from now also denoted as $aMCWD$) for 2005 and 2010, respectively, by first calculating the mean MCWD for the “baseline” period from 2000 to 2010 and second by subtracting the mean MCWD from 2005 and 2010, respectively. The $rMCWD$ anomaly is then estimated as the normalized deviation of the $aMCWD$ anomaly in units of standard deviation. The same procedure was applied for the $rMCWD$ anomaly for 2016, extending the baseline period from 2000 to 2016.

We define relative thresholds of $rMCWD$ anomaly < -0.5 as moderate, $rMCWD$ anomaly < -2.0 as severe, and $rMCWD < -2.5$ as extreme drought stress. Previously, levels of drought stress were based on $aMCWD$ anomaly (often also referred to as $\Delta MCWD$, e.g. Lewis et al. 2011) with $aMCWD$ anomaly $< -25 \text{ mm}$ as moderate drought stress because at this level, tree mortality already significantly increased in inventory plots.

186 By comparing empirical cumulative density functions of α MCWD and r MCWD anomalies (Fig. S1 and Methods S1) we are
187 also able to give absolute estimates for our relative thresholds with α MCWD < -26 mm, α MCWD < -106 mm, and
188 α MCWD < -132 mm reflecting moderate, severe and extreme drought stress, respectively. Choosing relative anomalies
189 over absolute enables a direct comparison of MCWD to the other drought indices used in this study. We used the r MCWD
190 anomaly every analysis conducted in our study. We also estimated seasonal patterns of cumulative water deficit (CWD), by
191 defining r CWD similar to r MCWD as the relative anomaly of each month's CWD in units of standard deviation.

192 2.3.2. Calculation of rainfall anomaly index (RAI)

194 For the rainfall anomaly index, dry season rainfall was taken as the mean precipitation from July-September following Lewis
195 et al. (2011). Like for the MCWD estimation, we calculated the mean dry season rainfall from a baseline period 2000-2010
196 to investigate the drought impacts of 2005 and 2010, and for 2016 we selected a baseline period from 2000 to 2016 excluding
197 2005, 2010, and 2016. The relative rainfall anomaly index (r RAI) was estimated as 'standardized anomaly' from the baseline
198 period similarly to the r MCWD anomaly calculation. As r RAI only reflects the precipitation anomaly during July and
199 September, it can also be described as a dry season anomaly.

200 2.3.3. Calculation of the self-calibrating Palmer Drought Severity Index (scPDSI)

202 The self-calibrating Palmer Drought Severity Index (scPDSI, Wells et al., 2004) has in recent studies been used to assess the
203 impacts of droughts on the Amazon basin (e.g. Jiménez-Muñoz et al., 2016). It improves the original PDSI by using a self-
204 calibrating procedure based on historical climate data, eliminating the empirically derived climatic characteristics. Next to
205 precipitation, it also takes monthly evapotranspiration ET into account. In our study, we use ET data generated from DOLCE
206 and GLEAM (section 2.4). Additionally, the scPDSI takes soil water capacity as input, which we assumed here as a constant
207 value of 100 mm. scPDSI was estimated using the R package *scPDSI* (Ruida et al., 2018).

208 To enable cross-comparison with the r MCWD and r RAI anomalies, we selected identical baseline periods from 2000 to 2010
209 for the 2005 and 2010 events, and from 2000 to 2016 for the 2016 drought event. Again, we used the relative deviation
210 r scPDSI, defined as 'standardized anomaly' from the baseline period of monthly scPDSI values as drought indicator.

211 2.4. Evapotranspiration datasets

212 In addition to assuming a constant evapotranspiration $ET(t) = ET_{fixed} = 100$ mm for the calculation of MCWD, and for the
213 calculation of scPDSI we use the two ET datasets GLEAM and DOLCE. The Global Land Evaporation Amsterdam Model
214 (GLEAM) v3a dataset (Martens et al., 2017) is derived from a set of algorithms incorporating satellite-observed soil moisture,
215 vegetation optical depth, reanalysis air temperature and radiation, and multiple precipitation datasets. The Derived Optimal
216 Linear Combination Evapotranspiration (DOLCE, Hobeichi et al., 2018) dataset is derived by combining and weighting
217 multiple other evapotranspiration datasets, also including GLEAM.

|
218
219
220
221
222
223
224
225
226
227
228
229
230
231

2.5. Calculation of drought area and extent

Each grid cell's area was approximated as a trapezoid to its boundary coordinates (in $0.5^\circ \times 0.5^\circ$ resolution), resulting in an area between 2900 and 3090 km² per grid cell. Accumulating the associated areas over all grid cells resulted in a total area of 5.94 million km² representing the Amazon Basin. Note that for comparison of our results with Lewis et al. (2011) differences in absolute areas arise because of differences in study area size (5.94 vs. 5.3 million km², respectively). For the calculation of the drought-affected area, we summed up the area of grid cells that matched the respective drought classification (e.g. *r*MCWD anomaly < -2.5 for extreme drought stress). The spatial agreement of drought location among datasets was estimated by selecting the grid cells matching the drought classification per dataset and subsequently counting the number of datasets per grid cells showing the respective drought classification.

3. Results

All areas in the following section are expressed as percentage with respect to the entire Amazon basin according to our delineation (5.94 million km²). For an overview of the areas affected in million km², see Tab. S1 and S2.

3.1 Comparison of total drought area based on relative MCWD anomaly

We first evaluate differences in $rMCWD$ for 2016 across the datasets (Fig. 1). Here, we find that the spatial patterns of the $rMCWD$ anomaly generally match across the available datasets, showing severe and extreme drought stress mainly in the northern Amazon basin. Only GLDAS diverges, showing extreme drought stress in the Central and Western part of Amazonia (Fig. 1d) where none of the other datasets shows any drought stress during the same year. The other datasets mostly differ regarding the intensity of the drought stress. While ERA5 and TRMM7 show values $rMCWD < -2.5$ in the Columbian part of the basin, CRUNCEP and GPCC do show such a strong drought impact only in Northern Brazil. The absolute areas of drought stress across different severity levels are similar across most datasets with only GLDAS showing a significantly larger area affected by extreme drought stress of $rMCWD < -2.5$.

Across all precipitation datasets, in 2005, an area ranging from 37 to 51% (mean 45%) of the whole Amazon basin, was moderately affected (Table S1, Fig. 2a). ERA5 displayed the smallest area affected by moderate drought (2.2 million km², Tab. 1, Fig. 2), while CHIRPS and CRUNCEP showed a vast affected area (3.0 million km²), an area about 36% larger than displayed by ERA5. For severe and extreme drought conditions, ERA5 shows the smallest affected area with 3% and 1% of the basin affected. For severe drought conditions, CRUNCEP suggests that an area approximately 3 times larger was affected compared to ERA5 (0.2 million km² vs. 0.6 million km²). CRUNCEP and GLDAS also encompass the largest area of extreme drought stress (0.2 million km²; 3% of the basin less than $rMCWD < -2.5$, Fig. 2a).

During the 2010 drought, a larger area ranging between a minimum of 52% (GPCC) and a maximum of 74% (TRMM 6) was affected by moderate drought stress, which is about 36% larger than during the 2005 drought (3.6 million km² vs. 2.7 million km², Table S1, Fig. 2). In addition, the area under severe drought stress was on average 25% larger compared to 2005 and the area affected by extreme drought was double the size of the 2005 drought event. Particularly, GLDAS and TRMM 6 showed the largest area affected throughout the three drought classifications (Fig. 2b).

For 2016, two datasets (CHIRPS and CRUNCEP) showed with 38% a considerably smaller area that was moderately affected by drought stress compared to GLDAS with 63% of the area affected, respectively (datasets ranging between 2.2 and 3.7 million km²). Generally, in 2016, the size of the area affected by moderate drought was in between the size of the area affected in 2005 and 2010, but the extent of severely and extremely drought-affected areas was larger. Here, particularly GLDAS followed by GPCC showed the largest affected area, with 21% severely affected and 6% extremely affected (Tab. S2).

3.2 Spatial agreement of rainfall datasets using the r MCWD anomaly

While the agreement of the total area affected by drought is relatively high (see 3.1) the data sets only partly agree on the spatial extent and location of extreme drought conditions, particularly during the 2010 and 2016 events (Fig. 3). For 2005, all datasets agree on the drought epicentre being in Central Amazonia. Datasets agree that an area of about 15 % of the Amazon Basin was at least moderately affected (Fig. 3a). Only a small overlap was found for the area affected by severe and extreme drought stress (Fig. 3b, c). Here, only half of the datasets agreed on 4% of central Amazonia being severely and 1.5% extremely affected.

For 2010, all datasets agreed on an affected area of 21% in the Amazon basin, and half of the datasets agreed on an area of 60% of the Amazon Basin being moderately affected by drought stress (Fig. 3d). The 2010 drought displayed no central hotspot, but three most affected areas in the Eastern, Southern and central parts of Amazonia on which most of the datasets agreed (Fig. 3d). Severe drought stress in 2010 was in the southern part of Amazonia, where four datasets agreed (Fig. 3e), while for extreme drought stress almost no overlap between datasets was found (Fig. 3f).

For 2016, all datasets agreed on an area of about 7% of moderate drought stress and half of the datasets agreed on 51% of the basin being affected (Fig. 3g). Agreement for severe and extreme drought stress was lower compared to the other drought years (Fig. 3h, i). Most of the datasets located the epicentre of the drought in the north-western Amazon basin. Some datasets also showed the South-Central part of the basin being severely affected (Fig. 3i).

We could not find any pronounced biases between the precipitation datasets (Fig. S3 - S5), but a generally higher correlation of the r MCWD anomalies for 2005 compared to 2010 and 2016. Only ERA5 and GLDAS showed some spikes in the r MCWD anomalies that are located within the high latitude regions of the Andes.

3.3 Constant versus varying evapotranspiration rates: Effects on drought severity and extent estimates

We find that assuming a constant ET rate of 100 mm month⁻¹ is only realistic in the Northern part of the Amazon basin and only when comparing to the DOLCE dataset (Fig. 4a, b), which shows ET rates of about 100mm month⁻¹ during both the wettest (as averaged between June to August) and the driest months (as averaged between January and March). Using GLEAM, average ET rates are between 30 and 50% higher than 100mm month⁻¹ during the wettest months (Fig. 4c) and remain higher than 100mm month⁻¹ also in the Northern part during the dry season (Fig. 4f). Evapotranspiration rates can be as low as 50mm month⁻¹ on average throughout the driest months for both ET datasets in the South of the basin (Fig. 4b. and 4f).

This spatial heterogeneity in evapotranspiration rates has implications for the extent and severity of drought stress expressed as r MCWD anomaly when compared to using constant evapotranspiration. Using the two evapotranspiration datasets we find lower drought impacts across most parts of the Amazon basin for the two years 2005 and 2010 (Fig. 4c, d, g, h). In 2005 the mean area of moderate drought stress is lower when using variable ET: 44% of the basin for GLEAM and 39% for DOLCE,

293 compared 46% for a constant ET. Interestingly, these differences were not particularly located in the epicentre of drought
294 during that year (see Fig. 3a, b, c), but rather in the South and the high latitude regions toward the Andes (Fig. 4c, g). The total
295 area of severe drought stress did only slightly decrease from 9% (constant ET) to 8% (GLEAM) and 7% (DOLCE). In 2010,
296 we find stronger differences between variable and constant ET. The area of moderate drought stress is 52% for GLEAM and
297 49% for DOLCE which is significantly lower than the 60% when using constant evapotranspiration. For this year the areas of
298 these differences (Fig. 4d, h) strongly overlap with the epicentres of the drought (see Fig. 3d, e, f). Consequently, also the areas
299 of severe drought stress are lower (7% for GLEAM, 8% for DOLCE) compared to using constant evapotranspiration (12%).
300 We find similar patterns for 2016 (not shown) where the mean area of severe drought stress is approximately 11% for both
301 GLEAM and DOLCE, which is lower compared to using constant ET (15%).

302 3.4 Comparison of drought indices: $rMCWD$, $rscPDSI$ and $rRAI$ anomalies

303 Similar to $rMCWD$, there is variable agreement among datasets when evaluating the other two drought metrics, $rRAI$ and
304 $rscPDSI$ (Fig. 5). The largest dry season anomaly ($rRAI$) in 2005 was displayed by GPCC with 6.5% (0.4 million km², Table
305 2), followed by TRMM 7 with 5.7% of the Amazon basin being severely affected. ERA 5 showed with 3% the smallest area
306 affected. In 2005, spatial patterns of $rRAI$ matched with $rMCWD$ anomalies despite $rMCWD$ anomalies showing a larger
307 area affected by severe drought stress (Fig. 5a, d). $rscPDSI$ displayed the smallest area affected by drought stress in 2005 with
308 also only GPCC and TRMM 7 showing with 5.5% and 3.1% the largest severely affected area, respectively. All other datasets
309 showed less than 1% of severe drought-affected areas in 2005. The small spatial area of $rscPDSI$ differed compared to the
310 other two drought indicators (Fig 5a, d, g): Some areas showed a strong disagreement between drought indices, e.g. Central
311 Amazonia was hit by severe drought stress according to $rMCWD$ and $rRAI$ (with 3-4 climate datasets in agreement) while,
312 in contrast, $rscPDSI$ did not indicate abnormally dry conditions there.

313 In 2010, the differences of drought-affected areas were even more pronounced between the three indices (Fig. 5b, e, h). Here,
314 ERA5 and TRMM7 showed the largest areas affected by severe drought stress based on the dry season $rRAI$ anomaly with
315 7% and 5%, respectively. Using $rscPDSI$ all datasets showed an area between 1% and 2.5% severely affected. Interestingly,
316 the area affected based on $rMCWD$ roughly encompasses the area affected by $rRAI$, but additionally shows a large area in the
317 South-Eastern part of the basin being affected by severe drought stress (Fig. 5b, e).

318 In 2016, $rscPDSI$ shows the largest area affected by drought stress with GLDAS showing 39% (followed by TRMM7, 16%)
319 of the basin being severely affected. Four datasets agreed on the affected area in the northeastern part of the basin (Fig. 5i).
320 Only one dataset (GLDAS) showed severe drought stress in 2016 when calculating dry season rainfall anomalies ($rRAI$, Fig

321 5c), indicating no pronounced anomalies in dry season rainfall according to all other datasets. $rMCWD$ and $rscPDSI$ roughly
322 agreed on the northern part of the basin being severely affected (Fig. 5f, i).

323 Average seasonal patterns are quite consistent across datasets but differ depending on the choice of drought index and drought
324 event (Fig. 6). The strongest (most negative) rainfall anomaly was visible from May to July during the 2005 drought event
325 (Fig. 6a). Accumulating such low rainfall estimates resulted in very low values of $rCWD$ during that period (Fig. 6d) in 2005.
326 $rscPDSI$ values were also low, but more constant throughout the year (Fig. 6g).

327 The 2010 drought followed similar patterns regarding $rRAI$ with a lower absolute impact during May to July compared to
328 2005 (Fig 6b). Interestingly, the wet season months March to May showed a strong anomaly during 2010 compared to the
329 2005 event. Subsequently, $rCWD$ was also already lower during the wet season in 2010 compared to 2005 (Fig. 6e). $rscPDSI$
330 anomalies values were similar for 2010 compared to 2005 with a slightly downward trend towards the end of the year (Fig.
331 6g, h).

332 To investigate the seasonal patterns of 2016 we also considered the drought indices of 2015 since both years were El Niño
333 years. We found a strong rainfall anomaly already starting during September 2015 continuing until April 2016 (Fig. 6c).
334 Consequently, also $rCWD$ values were very low during that period (Fig. 6f). While $rMCWD$ was applied as the maximum
335 value from October to September, drought stress before October of the previous year cannot be accounted for when using
336 $rMCWD$. The two-year drought impact was also visible using $scPDSI$ (Fig. 6i) showing a steady decline from 2015 to 2016.

337 **3.5 Overall variability: precipitation datasets vs. drought indices vs. evapotranspiration datasets**

338 When assessing the variability of drought severity and extent across the nine different precipitation datasets, the two drought
339 indices ($rMCWD$ and $rscPDSI$) and the two evapotranspiration datasets (DOLCE and GLEAM), we find that across all drought
340 events the choice of drought index accounts for roughly 60% of the variability while both the precipitation dataset and the
341 evapotranspiration dataset account for 20%, each (Tab. 2).

342

4. Discussion

We assessed the severity and spatial extent of the extreme drought years 2005, 2010, and 2015/2016 in the Amazon region by computing different drought indices using a range of precipitation datasets. When analyzing how drought conditions are captured in nine different precipitation datasets for the Amazon basin, we find that while the datasets mostly agree on the extent of the drought area, they differ in their location of drought.

Critical aspects regarding the detection of drought events in the Amazon basin

Drought indices

The idea of defining water deficit based on evapotranspiration rates goes back to Stephenson (1998) and the MCWD is now one of the most widely used indicators to assess drought stress in tropical forests (e.g. Lewis et al., 2011, Phillips et al., 2009, Esquivel-Muelbert et al., 2019). In its simplest form the calculation of MCWD only requires precipitation data and assumes a constant evapotranspiration (ET) rate of 100 mm month⁻¹ (Aragão et al., 2007). Although the simplicity of *r*MCWD and *a*MCWD is a main advantage, a fixed ET (which we also used in our study) is inappropriate for regions other than the lowland tropics, where the lower supply of energy may result in lower ET values. Most importantly, an approximated ET does not account for either seasonal variation (driven mainly by radiation, temperature, and phenology) or spatial variation in ET related to soil and root properties (Malhi et al., 2009). Hence, changes in *r*MCWD are purely accounting for changes in rainfall (Phillips et al., 2009). In contrast, *sc*PDSI is driven with spatially and temporally resolved evapotranspiration data. However, currently available evapotranspiration products for the Amazon rainforest show significant differences in areas and extent of evapotranspiration (Sörensson & Ruscica, 2018), hence introducing another source of uncertainty when using them for the calculation of drought indices. In the last decade, better products of spatially and temporally resolved evapotranspiration data (e.g. ERA5) have been developed and an increasing number of studies are now estimating MCWD based on such data (e.g. Staal et al., 2020). However, using a constant evapotranspiration (ET) rate of 100 mm month⁻¹ across the Amazon rainforest is still very common (e.g. Flack-Prain et al., 2019; Koch et al., 2021).

Using variable evapotranspiration consistently reduced the moderate drought-affected area by 5-10% per drought event (Fig. 4). Extending the baseline period of the MCWD calculation to include also years before 2001 leads to overall lower MCWD values and, hence, an increased intensity of the three drought events. This finding highlights the drought anomaly that the recent decade from 2001 to 2016 has compared to the years before that period.

The key difference between the three drought indices applied in our study is the temporal resolution: RAI is only calculated for the three driest months (July-September) and thus, for example, a rainy season with deficient rainfall is not captured. MCWD, in contrast, accumulates over 12 months and is reset to zero at the end of the hydrological year. In this way, drought events caused by low precipitation in both dry- and rainy seasons are captured, however, drought events lasting for more than a year are not detected. *sc*PDSI captures multi-year drought events and is not reset to zero at the end of the hydrological year.

376 These differences between the drought indicators can be seen for the three drought events analysed in this study. In 2005,
377 $rRAI$ and $rMCWD$ values roughly match in location of the epicenter indicating a particularly strong anomaly during the dry
378 season (Fig. 5a, d). This does not apply to the 2010 drought event, where despite some dry season anomaly an even stronger
379 anomaly during the wet season is visible (Fig. 6b, e). The 2015/2016 drought event is classified as a severe multi-year drought
380 according to Yang et al. (2018), which is also displayed in our analysis when using $rscPDSI$, (Fig 6i). $rMCWD$ and $rRAI$,
381 however, do not agree on a spatially and temporally extensive drought event in 2016 (Fig. 5c, f, i), but instead display distinct
382 regions of severe drought stress. Seasonal patterns of the three drought indices support this assumption (Fig. 6): Resetting
383 $rMCWD$ once per year neglects any influences of drought events of the preceding year (Fig. 6c). While the drought indices
384 used in this study showed pronounced differences in spatial and temporal dynamics, including all of them can help better
385 understanding the different characteristics that drought events can have in the Amazon basin.

386 A common drawback of all drought metrics used in our study is their incapability to explicitly represent the effect of increasing
387 atmospheric vapor pressure deficit (VPD) on plant water stress. A steady amplification of atmospheric vapor pressure deficit
388 (VPD) has been detected over the Amazon basin (Barkhordarian et al., 2019; Rifai et al., 2019). Such stronger atmospheric
389 water demand leads to additional water loss of plants during drought, subsequently increasing the severity of droughts. Hence,
390 the role of VPD during a drought and as a driver for plant stress should not be underestimated (Grossiord et al., 2020). With
391 increasing data availability and better estimates of VPD across the Amazon region, it should be included in future drought
392 assessments (e.g. Castro et al., 2020). One possibility to account for the influences of VPD is choosing temporal and spatially
393 resolved evapotranspiration instead of constant evapotranspiration in the calculation of MCWD. Future studies could further
394 investigate the relationships between MCWD, ET, and VPD and the impacts on biomass.

395 Furthermore, in the last decade, new methods have been developed that assess impacts of drought on ecosystems, e.g. analyses
396 based on solar-induced fluorescence (SIF) data show that tall forests are less sensitive to rainfall compared to short forests
397 (Giardina et al., 2018). Also, vegetation optical depth (VOD) used as a proxy for water content in forests is a promising
398 satellite-derived indicator for mortality and impacts of droughts on forests (Rao et al., 2019). However, conducting analyses
399 over the Amazon rainforest based on VOD is difficult, because of the limited penetration depth of microwaves in dense tropical
400 forests (Chaparro et al., 2019), and the influences of vegetation water status (Xu et al., 2021). So far, VOD data could only be
401 applied with limited success across tropical rainforests (Konings & Gentine, 2017). Future studies should estimate the impacts
402 of droughts based on multiple drought characteristics. For example, Toomey et al. (2011) show that considering both, heat
403 stress and soil moisture stress greatly improves the explanatory power of drought impacts in the Amazon basin.

405 *Precipitation datasets*

406 For the three drought events in 2005, 2010 and 2016, CHIRPS, GLDAS and ERA5 diverted the most from the other datasets
407 regarding the spatial drought extent. ERA5 shows the smallest area of moderate drought stress during 2005 but one of the
408 largest areas in 2010 (Fig. 2). We found no obvious bias between the precipitation datasets regarding distribution and frequency
409 of monthly rainfall (SI Fig. 2) with only ERA5 showing higher rainfall more frequently. Although TRMM7 and CHIRPS are

410 based on the same satellite data as their input, they differ regarding the size of the drought area, especially during 2016 (Fig.
411 2). Lewis et al. (2011) estimated an area of 47% (2.5 million km²) of the Amazon basin moderately affected in 2005 using the
412 TRMM6 dataset, which compares well with the size of the affected area for the majority of datasets analyzed in our study
413 (considering our 0.6 million km² larger study area; see Methods). For 2010, Lewis et al. (2011) reported an area of 3.2 million
414 km² being affected in comparison to 4.5 million km² in our analysis using TRMM6 with very similar spatial patterns. The
415 newer product, TRMM7, however, shows less frequent rainfall but heavier rainfall than CHIRPS maintaining a similar total
416 amount of precipitation (Giles et al., 2020). Also, both versions (TRMM6 and TRMM7) differ regarding the total area affected
417 by drought stress in 2005 and in particular in 2010, where TRMM6 showed a 10% larger area of the Amazon basin affected.
418 This can be explained by the generally higher precipitation rates detected in the TRMM7 dataset in comparison to TRMM6
419 (Seto et al., 2011) leading to lower absolute values of $rMCWD$. Spatially, this difference was most pronounced in the western
420 and northern parts of Amazonia, in the *Acre* and *Roraima* states, and in Peru. Because of such higher precipitation rates in
421 TRMM7 as compared to TRMM6, and subsequently the much stronger drought response according to our analysis, studies
422 based on TRMM6 only might overstate the actual drought conditions and should be revisited. Precipitation datasets usually
423 show remarkable differences in the representation of occurrence, frequency, intensity and location of events, mainly due to
424 their nature of high spatial and temporal variability (Covey et al., 2016; Dirmeyer et al., 2012). Generally, the sparse network
425 of observations in the Amazon rainforest may explain the differences across precipitation datasets and drought indices for
426 datasets that rely on station data. Within the last decade, the number of observations increased, due to a new denser network
427 of stations. This may improve the reanalysis models that are used for several precipitation datasets applied here, however, it
428 does not improve datasets that only rely on gauge observations. Bias-correction is also applied different across precipitation
429 datasets. So ~~do~~ CRUNCEP and WATCH WFDEI use two different gridded bias corrections inputs, while the simulated
430 precipitation fields of ERA5 are not using any bias corrections. Different datasets that are used for bias corrections can give
431 very different results on regional scales (Doblas-Reyes et al., 2021)

432 Jiménez-Muñoz et al. (2016) quantified drought extend using the scPDSI and found that 40%, 25% and 10% of the Amazon
433 basin were affected by moderate, severe, and extreme drought stress, respectively, in March 2016. While we did not evaluate
434 scPDSI directly but focused on $rscPDSI$ to allow for a better cross-comparison to the other drought indicators, we found
435 similar patterns for moderate drought stress (47% of the basin affected), but different patterns under severe (11%) and extreme
436 (1%) drought stress when evaluating $rscPDSI$ using the ERA5 dataset. Our estimation diverted from the results of Jiménez-
437 Muñoz et al. (2016) mainly because of our different drought classification, but also due to a different reference area (see
438 Methods).

439 In addition, Jiménez-Muñoz et al. (2016) used spatially resolved information on soil water capacity when calculating scPDSI
440 and a longer baseline period (year onset is 1979 in their study vs. 2000 in our study). Furthermore, the choice of the
441 precipitation dataset plays an important role. Compared to the datasets considered in our study, ERA 5 showed the weakest
442 drought impact during the 2016 drought event. GLDAS and TRMM7 showed a much stronger drought impact with over 70%
443 of the area moderately and between 15% and 39% severely affected (Tab. S2). This is particularly interesting because recent

445 studies identify TRMM7, CHIRPS and ERA5 as the best precipitation datasets when comparing to gauge observations in South
446 America (Albergel et al., 2018; Burton et al., 2018; Rifai et al., 2019). The higher scPDSI variability across the precipitation
447 datasets can be explained with the more complex algorithm (including the self-calibrating mechanism) the index has compared
448 to MCWD and RAI.

450 *Evapotranspiration datasets*

451 Using a variable ET dataset over constant ET of 100mm month⁻¹ leads to smaller areas affected by drought stress depending
452 on the year and drought location (Fig. 4). According to our findings using a constant ET of 100mm month⁻¹ introduces not
453 only a change in drought-affected areas, but rather a bias, as drought intensity and spatial extent are consistently higher for all
454 drought years. The reason for this bias lies within the calculation of MCWD which computes stronger deficits for higher values
455 of ET (e.g. 100 mm month⁻¹) than for lower values (e.g. 50 mm month⁻¹) during months with low precipitation. This bias can
456 be rather small during drought events that are located in the northern, wetter parts of the basin (as in 2005), but it can also be
457 quite strong for droughts that are located in the southern parts which have a more pronounced dry season (as in 2010).

459 **Implications for drought impact analyses in the Amazon rainforest**

460 Drought leads to increased tree mortality and carbon losses in tropical forests (Hubau et al., 2020; Lewis et al., 2011; Phillips
461 et al., 2009). With the prospect of more severe and frequent droughts in a future climate, more precise estimates of how much
462 carbon is lost from reductions in growth and drought-induced mortality are necessary. Currently, the Amazon rainforest is
463 acting as a carbon sink, thereby removing CO₂ from the atmosphere, but with more frequent and severe drought events, this
464 sink is already declining (Hubau et al. 2020). Lewis et al. (2011) estimated a total loss of biomass for the Amazon basin in
465 2005 of 1.6 Pg C and a 38% more severe impact of 2.2 PgC for 2010 based on TRMM6. Using TRMM7 instead of TRMM6
466 and using variable ET would likely decrease the impact of the 2010 drought on vegetation carbon as calculated in Lewis et al.
467 2011.

468
469 The affected areas (Fig. 2) for the drought events might be underestimated as (1) the total duration of the 2016 drought was
470 longer than 12 months (see above paragraph and Fig. 6) and can hence not be fully captured by the standard 12-month period
471 of the α MCWD and r MCWD calculation used in this study. (2) Potential lag effects due to delayed plant mortality within the
472 subsequent years are not considered so far. We would recommend for future studies to investigate the relationship of biomass
473 losses with other drought indices (such as scPDSI) in a similar manner as done in Lewis et al. (2011). As the biomass of the
474 Amazon rainforest is heterogeneously distributed (e.g. Saatchi et al., 2011), large-scale drought-induced biomass losses which
475 result from a severe α MCWD anomaly should be interpreted carefully. Differences in the amount of biomass in different forest
476 types, species composition, and critical hydraulic processes should be considered when estimating potential biomass losses
477 under drought stress (Feldpausch et al., 2016). A step forward would be to use, for example, remotely sensed biomass maps to
478 account for regional biomass distributions (e.g. Avitabile et al., 2016) or to simulate drought impacts with dynamic global

479 vegetation models (DGVMs). DGVMs simulate the carbon- and water cycle of the biosphere in a process-based way,
480 accounting for the interplay of carbon uptake and water loss through stomatal opening, evapotranspiration (ET), carbon
481 assimilation via photosynthesis, and carbon allocation to different plant compartments such as leaves, wood, and roots (e.g.
482 Schaphoff et al., 2018; Smith et al., 2014). The simulated response of tropical forests in DGVMs is particularly sensitive to
483 precipitation input under present and future climate change scenarios (e.g. Seiler et al., 2015). Therefore, we recommend using
484 multiple climate forcing datasets to test for climate data uncertainty also under present climate conditions. Particularly, studies
485 based on TRMM6 should possibly be revisited and complemented with more forcing datasets for their analysis.

487 6. Conclusions

488 We find substantial variation in the spatial extent, location, and timing of the extreme drought events in the years 2005, 2010
489 and 2016 in the Amazon basin. Depending on the precipitation dataset and drought index used, the area affected by severe
490 (extreme) drought varied between 0% and 39% (0% and 13.7%) for the 2016 event. Especially the area under severe drought
491 conditions changed from almost no severe drought stress (5 out of 6 datasets) when using $rRAI$ to greater than 10% when
492 using $rMCWD$ and $rscPDS$ instead. The variation partly results from the application of different drought metrics ($rMCWD$,
493 $rRAI$, $rscPDSI$) and from differences in the underlying precipitation datasets. Such differences also propagate when
494 quantifying the impacts of droughts on the carbon cycle of the Amazon rainforest and result in a large variability in biomass
495 carbon losses for a particular drought year. The estimated intensity of droughts depends predominantly on the selected drought
496 indicator and to a lesser extent on the choices of precipitation and evapotranspiration dataset.

497 We, therefore, recommend applying several drought metrics, climate (precipitation) datasets and, if available,
498 evapotranspiration datasets to account for model uncertainty when assessing the spatial extent, duration, and location of
499 droughts. We regard it as an important step when assessing drought impacts on tropical rainforests also under current climate
500 conditions. Communicating the uncertainty in the estimation of drought events and their impacts on the Amazon rainforest is
501 highly relevant and thus, multiple datasets should be applied by any large-scale study on drought impacts on vegetation.

503 7. Code availability

504 All scripts to reproduce analysis and figures are available at <https://github.com/PhillipPapastefanou/DroughtAnalysis>

505 8. Data availability

506 All datasets are available following the references in the method section.

508 9. Author contribution

509 P.P. and A.R. conceived the study and wrote the first draft of the manuscript. All authors contributed to the development of
510 the analysis and the writing of the manuscript.

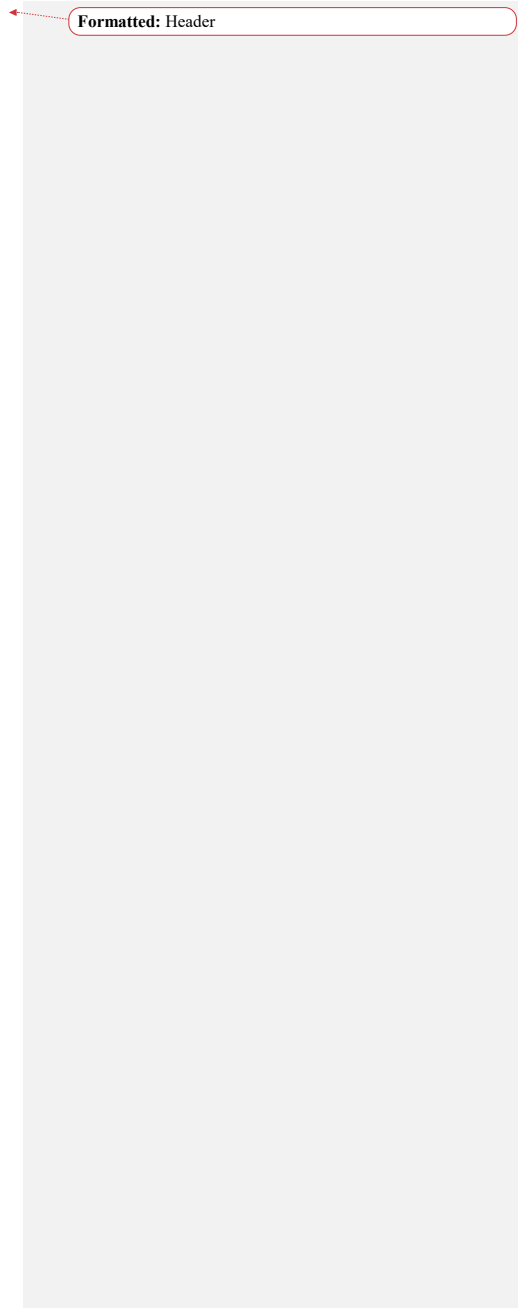
512 10. Competing interests

|

513 The authors declare no competing interests.

514

515



Formatted: Header

11. References

- 516 **11. References**
- 517 Albergel, C., Dutra, E., Munier, S., Calvet, J.-C., Munoz-Sabater, J., de Rosnay, P., & Balsamo, G. (2018). ERA-5 and ERA-
- 518 Interim driven ISBA land surface model simulations: Which one performs better? *Hydrology and Earth System*
- 519 *Sciences*, 22(6), 3515–3532. <https://doi.org/10.5194/hess-22-3515-2018>
- 520 Aragão, L. E. O. C., Malhi, Y., Roman-Cuesta, R. M., Saatchi, S., Anderson, L. O., & Shimabukuro, Y. E. (2007). Spatial
- 521 patterns and fire response of recent Amazonian droughts. *Geophysical Research Letters*, 34(7), L07701.
- 522 <https://doi.org/10.1029/2006GL028946>
- 523 Barkhordarian, A., Saatchi, S. S., Behrangi, A., Loikith, P. C., & Mechoso, C. R. (2019). A Recent Systematic Increase in
- 524 Vapor Pressure Deficit over Tropical South America. *Scientific Reports*, 9(1), 15331. [https://doi.org/10.1038/s41598-](https://doi.org/10.1038/s41598-019-51857-8)
- 525 [019-51857-8](https://doi.org/10.1038/s41598-019-51857-8)
- 526 Blacutt, L. A., Herdies, D. L., de Gonçalves, L. G. G., Vila, D. A., & Andrade, M. (2015). Precipitation comparison for the
- 527 CFSR, MERRA, TRMM3B42 and Combined Scheme datasets in Bolivia. *Atmospheric Research*, 163, 117–131.
- 528 <https://doi.org/10.1016/j.atmosres.2015.02.002>
- 529 Burton, C., Rifai, S., & Malhi, Y. (2018). Inter-comparison and assessment of gridded climate products over tropical forests
- 530 during the 2015/2016 El Niño. *Philosophical Transactions of the Royal Society B: Biological Sciences*, 373(1760),
- 531 20170406. <https://doi.org/10.1098/rstb.2017.0406>
- 532 Cai, W., Santoso, A., Wang, G., Yeh, S.-W., An, S.-I., Cobb, K. M., Collins, M., Guilyardi, E., Jin, F.-F., Kug, J.-S., Lengaigne,
- 533 M., McPhaden, M. J., Takahashi, K., Timmermann, A., Vecchi, G., Watanabe, M., & Wu, L. (2015). ENSO and
- 534 greenhouse warming. *Nature Climate Change*, 5(9), 849–859. <https://doi.org/10.1038/nclimate2743>
- 535 Castro, A. O., Chen, J., Zang, C. S., Shekhar, A., Jimenez, J. C., Bhattacharjee, S., Kindu, M., Morales, V. H., & Rammig, A.
- 536 (2020). OCO-2 Solar-Induced Chlorophyll Fluorescence Variability across Ecoregions of the Amazon Basin and the
- 537 Extreme Drought Effects of El Niño (2015–2016). *Remote Sensing*, 12(7), 1202–1202.
- 538 <https://doi.org/10.3390/rs12071202>

- 539 Chaparro, D., Duveiller, G., Piles, M., Cescatti, A., Vall-llossera, M., Camps, A., & Entekhabi, D. (2019). Sensitivity of L-
540 band vegetation optical depth to carbon stocks in tropical forests: A comparison to higher frequencies and optical
541 indices. *Remote Sensing of Environment*, 232, 111303. <https://doi.org/10.1016/j.rse.2019.111303>
- 542 Coelho, C. A. S., Cavalcanti, I. A. F., Costa, S. M. S., Freitas, S. R., Ito, E. R., Luz, G., Santos, A. F., Nobre, C. A., Marengo,
543 J. A., & Pezza, A. B. (2012). Climate diagnostics of three major drought events in the Amazon and illustrations of
544 their seasonal precipitation predictions. *Meteorological Applications*, 19(2), 237–255.
545 <https://doi.org/10.1002/met.1324>
- 546 Compo, G. P., Sardeshmukh, P. D., Whitaker, J. S., Brohan, P., Jones, P. D., & McColl, C. (2013). Independent confirmation
547 of global land warming without the use of station temperatures. *Geophysical Research Letters*, 40(12), 3170–3174.
548 <https://doi.org/10.1002/grl.50425>
- 549 Covey, C., Gleckler, P. J., Doutriaux, C., Williams, D. N., Dai, A., Fasullo, J., Trenberth, K., & Berg, A. (2016). Metrics for
550 the Diurnal Cycle of Precipitation: Toward Routine Benchmarks for Climate Models. *Journal of Climate*, 29(12),
551 4461–4471. <https://doi.org/10.1175/JCLI-D-15-0664.1>
- 552 da Rocha, H. R., Goulden, M. L., Miller, S. D., Menton, M. C., Pinto, L. D. V. O., de Freitas, H. C., & e Silva Figueira, A. M.
553 (2004). SEASONALITY OF WATER AND HEAT FLUXES OVER A TROPICAL FOREST IN EASTERN
554 AMAZONIA. *Ecological Applications*, 14(sp4), 22–32. <https://doi.org/10.1890/02-6001>
- 555 Dirmeyer, P. A., Cash, B. A., Kinter, J. L., Jung, T., Marx, L., Satoh, M., Stan, C., Tomita, H., Towers, P., Wedi, N.,
556 Achuthavarier, D., Adams, J. M., Altschuler, E. L., Huang, B., Jin, E. K., & Manganello, J. (2012). Simulating the
557 diurnal cycle of rainfall in global climate models: Resolution versus parameterization. *Climate Dynamics*, 39(1–2),
558 399–418. <https://doi.org/10.1007/s00382-011-1127-9>
- 559 Dirmeyer, P. A., Schlosser, C. A., & Brubaker, K. L. (2009). Precipitation, Recycling, and Land Memory: An Integrated
560 Analysis. *Journal of Hydrometeorology*, 10(1), 278–288. <https://doi.org/10.1175/2008JHM1016.1>
- 561 Doblas-Reyes, F. J., Sorensson, A. A., Almazroui, M., Dosio, A., Gutowski, W. J., Haarsma, R., Hamdi, R., Hewitson, B.,
562 Kwon, W.-T., Lamptey, B. L., Maraun, D., Stephenson, T. S., Takayabu, I., Terray, L., Turner, A., & Zuo, Z. (2021).
563 *Linking global to regional climate change* (V. Masson-Delmotte, P. Zhai, A. Pirani, S. L. Connors, C. Pean, S. Berger,

- 564 N. Caud, Y. Chen, L. Goldfarb, M. I. Gomis, M. Huang, K. Leitzell, E. Lonnoy, J. B. R. Matthews, T. K. Maycock,
565 T. Waterfield, O. Yelekci, R. Yu, & B. Zhou, Eds.). Cambridge University Press. <https://centaur.reading.ac.uk/99896/>
- 566 Döll, P., & Lehner, B. (2002). Validation of a new global 30-min drainage direction map. *Journal of Hydrology*, *258*(1–4),
567 214–231. [https://doi.org/10.1016/S0022-1694\(01\)00565-0](https://doi.org/10.1016/S0022-1694(01)00565-0)
- 568 Espinoza, J. C., Sörensson, A. A., Ronchail, J., Molina-Carpio, J., Segura, H., Gutierrez-Cori, O., Ruscica, R., Condom, T., &
569 Wongchuig-Correa, S. (2019). Regional hydro-climatic changes in the Southern Amazon Basin (Upper Madeira
570 Basin) during the 1982–2017 period. *Journal of Hydrology: Regional Studies*, *26*, 100637.
571 <https://doi.org/10.1016/j.ejrh.2019.100637>
- 572 Esquivel-Muelbert, A., Baker, T. R., Dexter, K. G., Lewis, S. L., Brienens, R. J. W., Feldpausch, T. R., Lloyd, J., Monteagudo-
573 Mendoza, A., Arroyo, L., Álvarez-Dávila, E., Higuchi, N., Marimon, B. S., Marimon-Junior, B. H., Silveira, M.,
574 Vilanova, E., Gloor, E., Malhi, Y., Chave, J., Barlow, J., ... Phillips, O. L. (2019). Compositional response of Amazon
575 forests to climate change. *Global Change Biology*, *25*(1), 39–56. <https://doi.org/10.1111/gcb.14413>
- 576 Feldpausch, T. R., Phillips, O. L., Brienens, R. J. W., Gloor, E., Lloyd, J., Lopez-Gonzalez, G., Monteagudo-Mendoza, A.,
577 Malhi, Y., Alarcón, A., Álvarez Dávila, E., Alvarez-Loayza, P., Andrade, A., Aragao, L. E. O. C., Arroyo, L., Aymard
578 C., G. A., Baker, T. R., Baraloto, C., Barroso, J., Bonal, D., ... Vos, V. A. (2016). Amazon forest response to repeated
579 droughts. *Global Biogeochemical Cycles*, *30*(7), 964–982. <https://doi.org/10.1002/2015GB005133>
- 580 Flack-Prain, S., Meir, P., Malhi, Y., Smallman, T. L., & Williams, M. (2019). The importance of physiological, structural and
581 trait responses to drought stress in driving spatial and temporal variation in GPP across Amazon forests.
582 *Biogeosciences*, *16*(22), 4463–4484. <https://doi.org/10.5194/bg-16-4463-2019>
- 583 Forkel, M., Drüke, M., Thurner, M., Dorigo, W., Schaphoff, S., Thonicke, K., von Bloh, W., & Carvalhais, N. (2019).
584 Constraining modelled global vegetation dynamics and carbon turnover using multiple satellite observations.
585 *Scientific Reports*, *9*(1), 18757. <https://doi.org/10.1038/s41598-019-55187-7>
- 586 Funk, C., Peterson, P., Landsfeld, M., Pedreros, D., Verdin, J., Shukla, S., Husak, G., Rowland, J., Harrison, L., Hoell, A., &
587 Michaelsen, J. (2015). The climate hazards infrared precipitation with stations—A new environmental record for
588 monitoring extremes. *Scientific Data*, *2*(1), 150066. <https://doi.org/10.1038/sdata.2015.66>

- 589 Giardina, F., Konings, A. G., Kennedy, D., Alemohammad, S. H., Oliveira, R. S., Uriarte, M., & Gentine, P. (2018). Tall
590 Amazonian forests are less sensitive to precipitation variability. *Nature Geoscience*, *11*(6), 405–409.
591 <https://doi.org/10.1038/s41561-018-0133-5>
- 592 Giles, J. A., Ruscica, R. C., & Menéndez, C. G. (2020). The diurnal cycle of precipitation over South America represented by
593 five gridded datasets. *International Journal of Climatology*, *40*(2), 668–686. <https://doi.org/10.1002/joc.6229>
- 594 Gloor, M., Barichivich, J., Ziv, G., Brienen, R., Schöngart, J., Peylin, P., Ladvocat Cintra, B. B., Feldpausch, T., Phillips, O.,
595 & Baker, J. (2015). Recent Amazon climate as background for possible ongoing and future changes of Amazon humid
596 forests. *Global Biogeochemical Cycles*, *29*(9), 1384–1399. <https://doi.org/10.1002/2014GB005080>
- 597 Golian, S., Javadian, M., & Behrangi, A. (2019). On the use of satellite, gauge, and reanalysis precipitation products for drought
598 studies. *Environmental Research Letters*, *14*(7), 075005. <https://doi.org/10.1088/1748-9326/ab2203>
- 599 Grossiord, C., Buckley, T. N., Cernusak, L. A., Novick, K. A., Poulter, B., Siegwolf, R. T. W., Sperry, J. S., & McDowell, N.
600 G. (2020). Plant responses to rising vapor pressure deficit. *New Phytologist*, *226*(6), 1550–1566.
601 <https://doi.org/10.1111/nph.16485>
- 602 Harris, I., Jones, P. D., Osborn, T. J., & Lister, D. H. (2014). Updated high-resolution grids of monthly climatic observations
603 - the CRU TS3.10 Dataset: UPDATED HIGH-RESOLUTION GRIDS OF MONTHLY CLIMATIC
604 OBSERVATIONS. *International Journal of Climatology*, *34*(3), 623–642. <https://doi.org/10.1002/joc.3711>
- 605 Hobeichi, S., Abramowitz, G., Evans, J., & Ukkola, A. (2018). Derived Optimal Linear Combination Evapotranspiration
606 (DOLCE): A global gridded synthesis ET estimate. *Hydrology and Earth System Sciences*, *22*(2), 1317–1336.
607 <https://doi.org/10.5194/hess-22-1317-2018>
- 608 Hubau, W., Lewis, S. L., Phillips, O. L., Affum-Baffoe, K., Beeckman, H., Cuni-Sanchez, A., Daniels, A. K., Ewango, C. E.
609 N., Fauset, S., Mukinzi, J. M., Sheil, D., Sonké, B., Sullivan, M. J. P., Sunderland, T. C. H., Taedoumg, H., Thomas,
610 S. C., White, L. J. T., Abernethy, K. A., Adu-Bredu, S., ... Zemagho, L. (2020). Asynchronous carbon sink saturation
611 in African and Amazonian tropical forests. *Nature*, *579*(7797), 80–87. <https://doi.org/10.1038/s41586-020-2035-0>

- 612 Huffman, G. J., Bolvin, D. T., Nelkin, E. J., Wolff, D. B., Adler, R. F., Gu, G., Hong, Y., Bowman, K. P., & Stocker, E. F.
613 (2007). The TRMM Multisatellite Precipitation Analysis (TMPA): Quasi-Global, Multiyear, Combined-Sensor
614 Precipitation Estimates at Fine Scales. *Journal of Hydrometeorology*, 8(1), 38–55. <https://doi.org/10.1175/JHM560.1>
- 615 Jiang, M., Medlyn, B. E., Drake, J. E., Duursma, R. A., Anderson, I. C., Barton, C. V. M., Boer, M. M., Carrillo, Y., Castañeda-
616 Gómez, L., Collins, L., Crous, K. Y., De Kauwe, M. G., dos Santos, B. M., Emmerson, K. M., Facey, S. L., Gherlenda,
617 A. N., Gimeno, T. E., Hasegawa, S., Johnson, S. N., ... Ellsworth, D. S. (2020). The fate of carbon in a mature forest
618 under carbon dioxide enrichment. *Nature*, 580(7802), 227–231. <https://doi.org/10.1038/s41586-020-2128-9>
- 619 Jimenez, J. C., Barichivich, J., Mattar, C., Takahashi, K., Santamaria-Artigas, A., Sobrino, J. A., & Malhi, Y. (2018). Spatio-
620 temporal patterns of thermal anomalies and drought over tropical forests driven by recent extreme climatic anomalies.
621 *Philosophical Transactions of the Royal Society B: Biological Sciences*, 373(1760), 20170300.
622 <https://doi.org/10.1098/rstb.2017.0300>
- 623 Jimenez, J. C., Marengo, J. A., Alves, L. M., Sulca, J. C., Takahashi, K., Ferrett, S., & Collins, M. (2019). The role of ENSO
624 flavours and TNA on recent droughts over Amazon forests and the Northeast Brazil region. *International Journal of*
625 *Climatology*, 41(7), 3761–3780. <https://doi.org/10.1002/joc.6453>
- 626 Jiménez-Muñoz, J. C., Mattar, C., Barichivich, J., Santamaria-Artigas, A., Takahashi, K., Malhi, Y., Sobrino, J. A., & Schrier,
627 G. van der. (2016). Record-breaking warming and extreme drought in the Amazon rainforest during the course of El
628 Niño 2015–2016. *Scientific Reports*, 6(1), 33130. <https://doi.org/10.1038/srep33130>
- 629 Koch, A., Hubau, W., & Lewis, S. L. (2021). Earth System Models Are Not Capturing Present-Day Tropical Forest Carbon
630 Dynamics. *Earth's Future*, 9(5). <https://doi.org/10.1029/2020EF001874>
- 631 Konings, A. G., & Gentine, P. (2017). Global variations in ecosystem-scale isohydricity. *Global Change Biology*, 23(2), 891–
632 905. <https://doi.org/10.1111/gcb.13389>
- 633 Lewis, S. L., Brando, P. M., Phillips, O. L., van der Heijden, G. M. F., & Nepstad, D. (2011). The 2010 Amazon Drought.
634 *Science*, 331(6017), 554–554. <https://doi.org/10.1126/science.1200807>

- 635 Malhi, Y., Aragao, L. E. O. C., Galbraith, D., Huntingford, C., Fisher, R., Zelazowski, P., Sitch, S., McSweeney, C., & Meir,
636 P. (2009). Exploring the likelihood and mechanism of a climate-change-induced dieback of the Amazon rainforest.
637 *Proceedings of the National Academy of Sciences*, 106(49), 20610–20615. <https://doi.org/10.1073/pnas.0804619106>
- 638 Malhi, Y., Roberts, J. T., Betts, R. A., Killeen, T. J., Li, W., & Nobre, C. A. (2008). Climate Change, Deforestation, and the
639 Fate of the Amazon. *Science*, 319(5860), 169–172. <https://doi.org/10.1126/science.1146961>
- 640 Marengo, J. A., & Espinoza, J. C. (2016). Extreme seasonal droughts and floods in Amazonia: Causes, trends and impacts:
641 EXTREMES IN AMAZONIA. *International Journal of Climatology*, 36(3), 1033–1050.
642 <https://doi.org/10.1002/joc.4420>
- 643 Marengo, J. A., Nobre, C. A., Tomasella, J., Cardoso, M. F., & Oyama, M. D. (2008). Hydro-climatic and ecological behaviour
644 of the drought of Amazonia in 2005. *Philosophical Transactions of the Royal Society B: Biological Sciences*,
645 363(1498), 1773–1778. <https://doi.org/10.1098/rstb.2007.0015>
- 646 Marengo, J. A., Nobre, C. A., Tomasella, J., Oyama, M. D., Sampaio de Oliveira, G., de Oliveira, R., Camargo, H., Alves, L.
647 M., & Brown, I. F. (2008). The Drought of Amazonia in 2005. *Journal of Climate*, 21(3), 495–516.
648 <https://doi.org/10.1175/2007JCLI1600.1>
- 649 Marengo, J. A., Tomasella, J., Alves, L. M., Soares, W. R., & Rodriguez, D. A. (2011). The drought of 2010 in the context of
650 historical droughts in the Amazon region: DROUGHT AMAZON 2010. *Geophysical Research Letters*, 38(12), n/a-
651 n/a. <https://doi.org/10.1029/2011GL047436>
- 652 Martens, B., Miralles, D. G., Lievens, H., van der Schalie, R., de Jeu, R. A. M., Fernández-Prieto, D., Beck, H. E., Dorigo, W.
653 A., & Verhoest, N. E. C. (2017). GLEAM v3: Satellite-based land evaporation and root-zone soil moisture.
654 *Geoscientific Model Development*, 10(5), 1903–1925. <https://doi.org/10.5194/gmd-10-1903-2017>
- 655 Miralles, D. G., Gentile, P., Seneviratne, S. I., & Teuling, A. J. (2019). Land-atmospheric feedbacks during droughts and
656 heatwaves: State of the science and current challenges: Land feedbacks during droughts and heatwaves. *Annals of the
657 New York Academy of Sciences*, 1436(1), 19–35. <https://doi.org/10.1111/nyas.13912>
- 658 Muñoz-Sabater, J., Dutra, E., Balsamo, G., Boussetta, S., Zsoter, E., Albergel, C., & Agustí-Panareda, A. (2018). *ERA5-Land:
659 An improved version of the ERA5 reanalysis land component.*

- 660 Nogueira, M. (2020). Inter-comparison of ERA-5, ERA-interim and GPCP rainfall over the last 40 years: Process-based
661 analysis of systematic and random differences. *Journal of Hydrology*, 583, 124632.
662 <https://doi.org/10.1016/j.jhydrol.2020.124632>
- 663 Phillips, O. L., Aragão, L. E. O. C., Lewis, S. L., Fisher, J. B., Lloyd, J., López-González, G., Malhi, Y., Monteagudo, A.,
664 Peacock, J., Quesada, C. A., van der Heijden, G., Almeida, S., Amaral, I., Arroyo, L., Aymard, G., Baker, T. R.,
665 Bánki, O., Blanc, L., Bonal, D., ... Torres-Lezama, A. (2009). Drought Sensitivity of the Amazon Rainforest. *Science*,
666 323(5919), 1344–1347. <https://doi.org/10.1126/science.1164033>
- 667 Rao, K., Anderegg, W. R. L., Sala, A., Martínez-Vilalta, J., & Konings, A. G. (2019). Satellite-based vegetation optical depth
668 as an indicator of drought-driven tree mortality. *Remote Sensing of Environment*, 227, 125–136.
669 <https://doi.org/10.1016/j.rse.2019.03.026>
- 670 Rifai, S. W., Li, S., & Malhi, Y. (2019). Coupling of El Niño events and long-term warming leads to pervasive climate extremes
671 in the terrestrial tropics. *Environmental Research Letters*, 14(10), 105002. <https://doi.org/10.1088/1748-9326/ab402f>
- 672 Rodell, M., Houser, P. R., Jambor, U., Gottschalck, J., Mitchell, K., Meng, C.-J., Arsenault, K., Cosgrove, B., Radakovich, J.,
673 Bosilovich, M., Entin, J. K., Walker, J. P., Lohmann, D., & Toll, D. (2004). The Global Land Data Assimilation
674 System. *Bulletin of the American Meteorological Society*, 85(3), 381–394. <https://doi.org/10.1175/BAMS-85-3-381>
- 675 Ruida, Z., Chen, X., Wang, Z., Lai, C., & Goddard, S. (2018). *Package scPDSI*. <https://github.com/Sibada/scPDSI>
- 676 Schneider, U., Becker, A., Finger, P., Anja, M.-C., & Markus, Z. (2018). *GPCC Full Data Monthly Version 2018.0 at 0.5°:*
677 *Monthly Land-Surface Precipitation from Rain-Gauges built on GTS-based and Historic Data.*
678 https://doi.org/10.5676/DWD_GPCC/FD_M_V2018_050
- 679 Seto, S., Iguchi, T., & Meneghini, R. (2011). Comparison of TRMM PR V6 and V7 focusing heavy rainfall. *2011 IEEE*
680 *International Geoscience and Remote Sensing Symposium*, 2582–2585.
681 <https://doi.org/10.1109/IGARSS.2011.6049769>
- 682 Sheffield, J., Goteti, G., & Wood, E. F. (2006). Development of a 50-Year High-Resolution Global Dataset of Meteorological
683 Forcings for Land Surface Modeling. *Journal of Climate*, 19(13), 3088–3111. <https://doi.org/10.1175/JCLI3790.1>

- 684 Sörensson, A. A., & Ruscica, R. C. (2018). Intercomparison and Uncertainty Assessment of Nine Evapotranspiration Estimates
685 Over South America. *Water Resources Research*, 54(4), 2891–2908. <https://doi.org/10.1002/2017WR021682>
- 686 Staal, A., Fetzer, I., Wang-Erlandsson, L., Bosmans, J. H. C., Dekker, S. C., van Nes, E. H., Rockström, J., & Tuinenburg, O.
687 A. (2020). Hysteresis of tropical forests in the 21st century. *Nature Communications*, 11(1), 4978.
688 <https://doi.org/10.1038/s41467-020-18728-7>
- 689 Toomey, M., Roberts, D. A., Still, C., Goulden, M. L., & McFadden, J. P. (2011). Remotely sensed heat anomalies linked with
690 Amazonian forest biomass declines: AMAZON DROUGHT THERMAL ANOMALIES. *Geophysical Research
691 Letters*, 38(19), n/a-n/a. <https://doi.org/10.1029/2011GL049041>
- 692 van der Ent, R. J., Savenije, H. H. G., Schaeffli, B., & Steele-Dunne, S. C. (2010). Origin and fate of atmospheric moisture
693 over continents: ORIGIN AND FATE OF ATMOSPHERIC MOISTURE. *Water Resources Research*, 46(9).
694 <https://doi.org/10.1029/2010WR009127>
- 695 Viovy, N. (2018). *CRUNCEP Version 7—Atmospheric Forcing Data for the Community Land Model*.
696 <http://rda.ucar.edu/datasets/ds314.3/%22>
- 697 von Randow, C., Manzi, A. O., Kruijt, B., de Oliveira, P. J., Zanchi, F. B., Silva, R. L., Hodnett, M. G., Gash, J. H. C., Elbers,
698 J. A., Waterloo, M. J., Cardoso, F. L., & Kabat, P. (2004). Comparative measurements and seasonal variations in
699 energy and carbon exchange over forest and pasture in South West Amazonia. *Theoretical and Applied Climatology*,
700 78(1–3). <https://doi.org/10.1007/s00704-004-0041-z>
- 701 Weedon, G. P., Balsamo, G., Bellouin, N., Gomes, S., Best, M. J., & Viterbo, P. (2014). The WFDEI meteorological forcing
702 data set: WATCH Forcing Data methodology applied to ERA-Interim reanalysis data. *Water Resources Research*,
703 50(9), 7505–7514. <https://doi.org/10.1002/2014WR015638>
- 704 Weedon, G. P., Gomes, S., Viterbo, P., Shuttleworth, W. J., Blyth, E., Österle, H., Adam, J. C., Bellouin, N., Boucher, O., &
705 Best, M. (2011). Creation of the WATCH Forcing Data and Its Use to Assess Global and Regional Reference Crop
706 Evaporation over Land during the Twentieth Century. *Journal of Hydrometeorology*, 12(5), 823–848.
707 <https://doi.org/10.1175/2011JHM1369.1>

- 708 Wells, N., Goddard, S., & Hayes, M. J. (2004). A Self-Calibrating Palmer Drought Severity Index. *Journal of Climate*, *17*(12),
709 2335–2351. [https://doi.org/10.1175/1520-0442\(2004\)017<2335:ASPDSI>2.0.CO;2](https://doi.org/10.1175/1520-0442(2004)017<2335:ASPDSI>2.0.CO;2)
- 710 Willmott, C. J., Rowe, C. M., & Philpot, W. D. (1985). Small-Scale Climate Maps: A Sensitivity Analysis of Some Common
711 Assumptions Associated with Grid-Point Interpolation and Contouring. *The American Cartographer*, *12*(1), 5–16.
712 <https://doi.org/10.1559/152304085783914686>
- 713 Xu, X., Konings, A. G., Longo, M., Feldman, A., Xu, L., Saatchi, S., Wu, D., Wu, J., & Moorcroft, P. (2021). Leaf surface
714 water, not plant water stress, drives diurnal variation in tropical forest canopy water content. *New Phytologist*, *231*(1),
715 122–136. <https://doi.org/10.1111/nph.17254>
- 716 Yang, H., Piao, S., Zeng, Z., Ciais, P., Yin, Y., Friedlingstein, P., Sitch, S., Ahlström, A., Guimberteau, M., Huntingford, C.,
717 Levis, S., Levy, P. E., Huang, M., Li, Y., Li, X., Lomas, M. R., Peylin, P., Poulter, B., Viovy, N., ... Wang, L. (2015).
718 Multicriteria evaluation of discharge simulation in Dynamic Global Vegetation Models. *Journal of Geophysical*
719 *Research: Atmospheres*, *120*(15), 7488–7505. <https://doi.org/10.1002/2015JD023129>
- 720 Yang, Y., Saatchi, S. S., Xu, L., Yu, Y., Choi, S., Phillips, N., Kennedy, R., Keller, M., Knyazikhin, Y., & Myneni, R. B.
721 (2018). Post-drought decline of the Amazon carbon sink. *Nature Communications*, *9*(1), 3172.
722 <https://doi.org/10.1038/s41467-018-05668-6>
- 723 Zang, C. S., Buras, A., Esquivel-Muelbert, A., Jump, A. S., Rigling, A., & Rammig, A. (2020). Standardized drought indices
724 in ecological research: Why one size does not fit all. *Global Change Biology*, *26*(2), 322–324.
725 <https://doi.org/10.1111/gcb.14809>
- 726 Zemp, D. C., Schleussner, C.-F., Barbosa, H. M. J., Hirota, M., Montade, V., Sampaio, G., Staal, A., Wang-Erlandsson, L., &
727 Rammig, A. (2017). Self-amplified Amazon forest loss due to vegetation-atmosphere feedbacks. *Nature*
728 *Communications*, *8*(1), 14681. <https://doi.org/10.1038/ncomms14681>
- 729 Zemp, D. C., Schleussner, C.-F., Barbosa, H. M. J., van der Ent, R. J., Donges, J. F., Heinke, J., Sampaio, G., & Rammig, A.
730 (2014). On the importance of cascading moisture recycling in South America. *Atmospheric Chemistry and Physics*,
731 *14*(23), 13337–13359. <https://doi.org/10.5194/acp-14-13337-2014>

- 732 Zeng, N., Yoon, J.-H., Marengo, J. A., Subramaniam, A., Nobre, C. A., Mariotti, A., & Neelin, J. D. (2008). Causes and
733 impacts of the 2005 Amazon drought. *Environmental Research Letters*, 3(1), 014002. [https://doi.org/10.1088/1748-](https://doi.org/10.1088/1748-9326/3/1/014002)
734 [9326/3/1/014002](https://doi.org/10.1088/1748-9326/3/1/014002)
- 735 Ziese, M., Schneider, U., Meyer-Christoffer, A., Schamm, K., Vido, J., Finger, P., Bissolli, P., Pietzsch, S., & Becker, A.
736 (2014). The GPCP Drought Index – a new, combined and gridded global drought index. *Earth System Science Data*,
737 6(2), 285–295. <https://doi.org/10.5194/essd-6-285-2014>

738
739
740
741

Precipitation dataset	Abbreviation	Details	Resolutions	Derived from	References
Climate Hazards group Infrared Precipitation with Stations	CHIRPS	quasi-global (50°S-50°N)	high resolution (0.05°), daily, pentadal, and monthly	Remote sensing, in-situ observations	Funk et al., 2015
Tropical Rainfall Measurement Mission	TRMM v6 3b43	quasi-global (50°S-50°N)	Quarter degree resolution (0.25°) daily, pentadal, and monthly	Remote sensing	Huffman et al., 2007
Tropical Rainfall Measurement Mission	TRMM v7 3B43	quasi-global (50°S-50°N)	Quarter degree resolution (0.25°), daily, pentadal, and monthly	Remote sensing	Huffman et al., 2007
	CRU_NCEP V8	global	Half degree resolution (0.5°), daily, pentadal and monthly	Reanalysis corrected by CRU gridded observational dataset	Viovy et al., 2017
ERA5		global	Quarter degree resolution (0.25°), sub-daily, daily, monthly	Reanalysis	Albergel et al., 2018
Global Land Data Assimilation System	GLDAS 2.1	global	Quarter degree resolution (0.25°), daily, pentadal, and monthly	Geostationary satellite infrared cloud-top temperature	Rodell et al., 2004

Formatted: Header

Formatted Table

				measurements and microwave observation techniques.	
Global Precipitation Climatology Centre at Deutscher Wetterdienst	GPCC2018	global	Quarter degree resolution (0.25°), monthly	Gridded in-situ observations	Schneider et al., 2018
Global Soil Wetness Project Phase 3	GSWP3	global	Half degree resolution (0.5°), daily, monthly	Reanalysis (20CR) corrected with gridded observation (GPCC)	H. Kim et al. n.d.;
WATCH Forcing Data (WFD) + WATCH Forcing Data methodology applied to ERA-Interim data (WFDEI)	WATCH_WFDEI	global	Half degree resolution (0.5°), daily, monthly	Hydrological model applied to ERA_Interim data	Weedon et al., 2011, 2014

743 **Table 1: Overview of the 10 precipitation datasets used in our study. Columns show the name of the dataset, the official**
744 **abbreviation, the short abbreviation used in here, the spatial and temporal resolution and the references.**

745

746

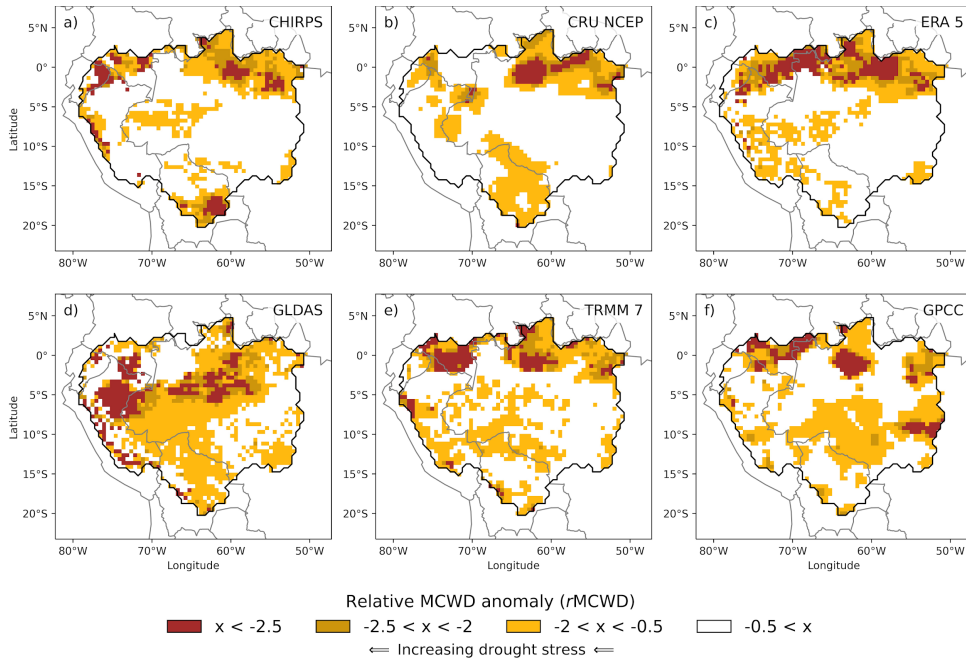
747

Formatted: Header

Drought event	Fraction of overall variability in rMCWD anomaly based on		
	precipitation datasets	drought indicators	evapotranspiration datasets
2005	0.21	0.6	0.19
2010	0.21	0.58	0.21
2016	0.22	0.59	0.19

Table 2: Fraction of overall variability in rMCWD anomaly based on precipitation datasets, drought indicators, and evapotranspiration datasets.

748
749
750

751 **Figures**

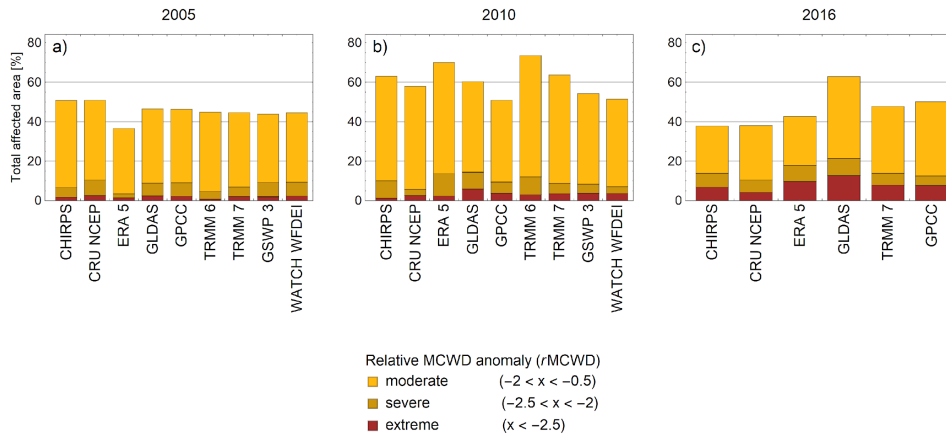
752

753 **Figure 1: Relative MCWD anomalies (from October to September) as an indicator for drought stress in the Amazon**
 754 **basin during the record-breaking drought event in 2016. Displayed are only the datasets that include the year 2016 in**
 755 **their temporal range. The baseline period of the MCWD calculation is 2001 to 2016.**

756

757

758
759



760
761

762 **Figure 2: Total area of the Amazon basin affected by drought stress (%) according to relative MCWD anomaly for**
763 **each of the precipitation datasets. Displayed are the three drought events (a) 2005, (b) 2010 and (c) 2016. The total**
764 **area representing the Amazon basin in our study is 5.94 million km². For absolute area affected, see Tab. S2 and S3.**

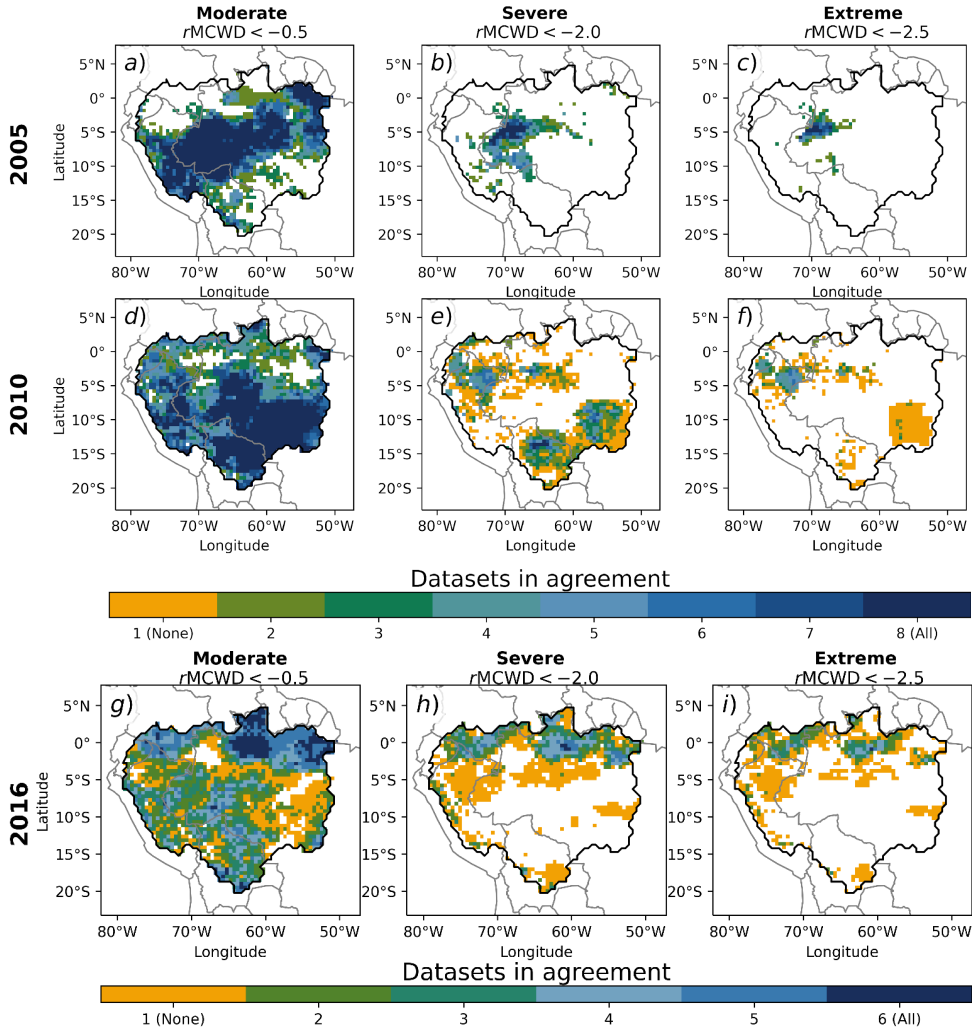
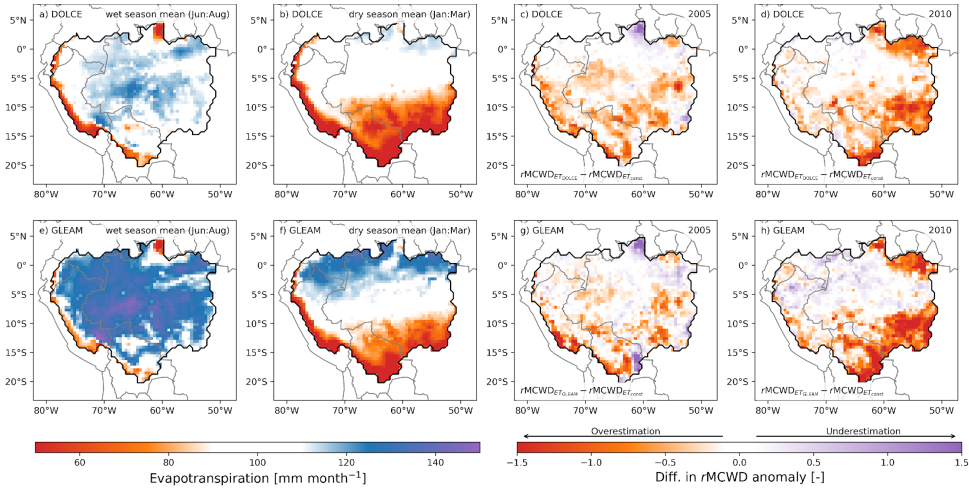


Figure 3: Agreement of precipitation datasets on drought area as identified by relative MCWD anomalies. In columns, different levels of drought severity are displayed and rows show the different drought years 2005 (a-c), 2010 (d-f) and

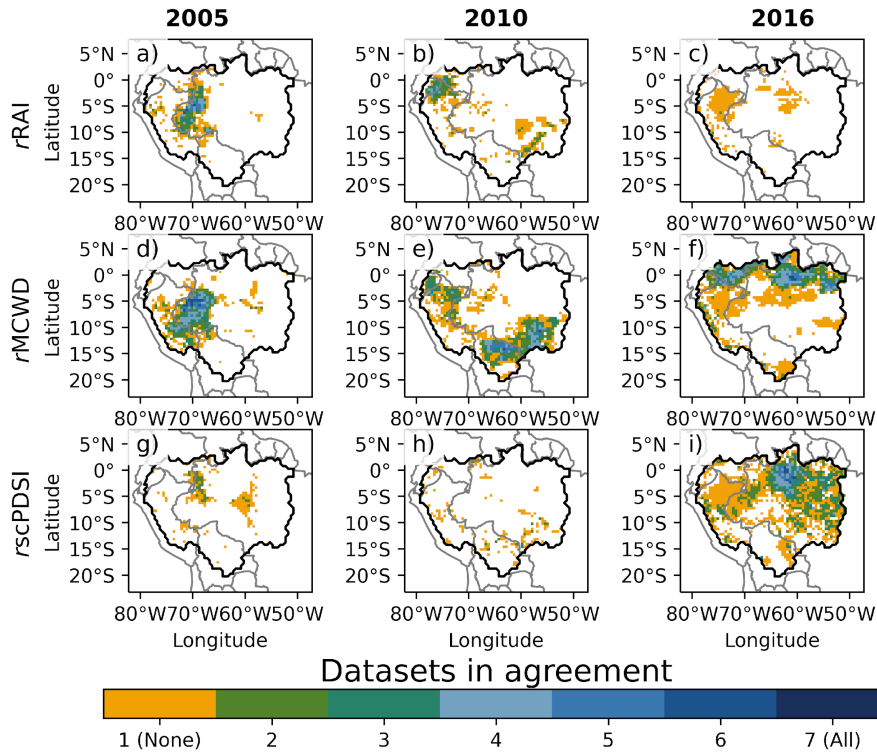
|
770
771
772
773
774
775
776

2016 (g-i). The colors indicate the number of datasets that agree on a specific drought level in a given pixel. Drought severity levels are defined as moderate ($rMCWD < -0.5$), severe ($rMCWD < -2.0$) and extreme ($rMCWD < -2.5$). Orange pixels indicate areas where only one dataset shows the respective drought stress (No agreement = “None”). White pixels represent areas where no dataset shows any drought signal. Note that in a-f, TRMM 6 and GSWP3 were excluded, as they were either very similar to its successor (TRMM 7) or due to a similar reanalysis procedure (WATCH_WFDEI). In g-i, only six datasets were included, which cover the full time period until 2016.

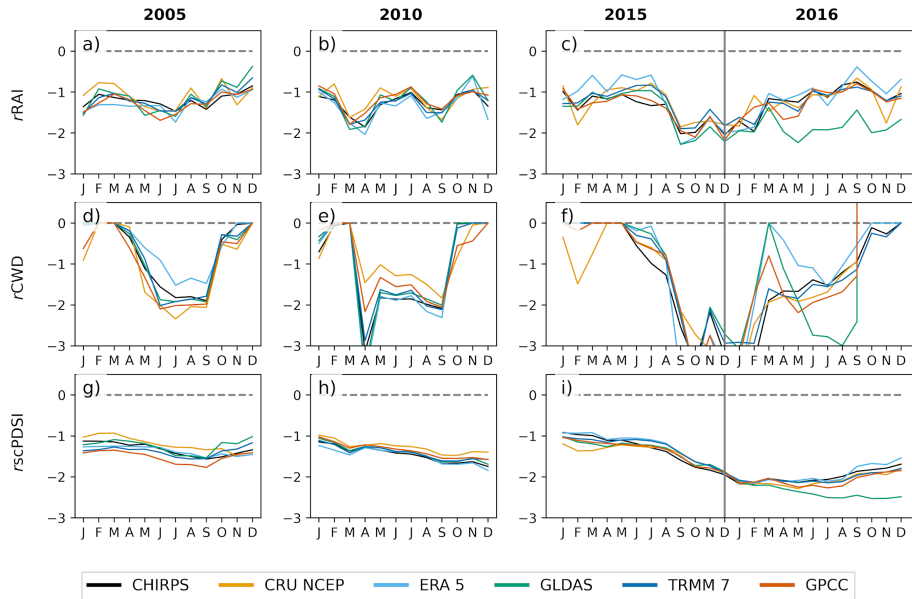
Formatted: Header



778
 779 **Figure 4: Spatial pattern of ET for the dry and wet season for the DOLCE and GLEAM datasets (a, b, e, f) and**
 780 **the differences between using the two ET datasets to calculate the rMCWD anomaly and the rMCWD based on the constant**
 781 **ET=100mm per month assumption for 2005 (c, g) and 2010 (d, h). Wet and dry season ET is calculated as mean from**
 782 **June to August and January and March, respectively. Negative (positive) differences of the rMCWD anomalies indicate**
 783 **an overestimation (underestimation) of drought stress when using ET=100mm per month compared to the respective**
 784 **evapotranspiration dataset.**



790 **Figure 5: Agreement of precipitation datasets on drought area as identified by different drought metrics. Comparison**
 791 **of the Amazon drought events in 2005, 2010 and 2016 (columns) vs three different drought indexes (rows): r MCWD**
 792 **(a-c), r scPDSI (d-f) and r RAI (g-i). Only the area affected by severe drought stress is displayed, which is defined equally**
 793 **for each of the drought indices. Orange pixels indicate areas where only one dataset shows the respective drought stress**
 794 **(“None”). White pixels represent areas where no dataset shows any drought signal.**
 795



797 **Figure 6: Monthly development of the Amazon drought events in 2005, 2010 and 2016 (columns) as described by the**
 798 **three different drought indices (rows): $rMCWD$ (a-c), $rscPDSI$ (d-f) and relative rainfall anomaly ($rRAI$, g-i).** Colored
 799 **lines indicate the indices of the 10% quantile of all gridcells of each of the different precipitation datasets. The indices**
 800 **are estimated as relative deviation from a 2001 to 2016 baseline period for each month.**
 801
 802
 803